

ARTICLE

Synergetic effect of aramid nanofiber-graphene oxide hybrid filler on the properties of rubber compounds for tire tread application

Jaehyun Jung^{1,2}  | Henry A. Sodano^{1,3,4} 

¹Department of Macromolecular Science and Engineering, University of Michigan, Ann Arbor, Michigan, USA

²R&D Center, Hankook Tire and Technology Co., Ltd, Daejeon, South Korea

³Department of Aerospace Engineering, University of Michigan, Ann Arbor, Michigan, USA

⁴Department of Materials Science and Engineering, University of Michigan, Ann Arbor, Michigan, USA

Correspondence

Henry A. Sodano, Department of Aerospace Engineering, University of Michigan, Ann Arbor, MI 48109, USA.
Email: hsodano@umich.edu

Funding information

Air Force Office of Scientific Research, Grant/Award Number: FA9550-21-1-0019; Army Research Office, Grant/Award Number: W911NF-18-1-0061; Hankook Tire and Technology

Abstract

The properties of rubber compounds used in tire tread largely contribute to the overall performance of tires in vehicles. Among the various ingredients used, reinforcing fillers are known for having the most significant effect on the static and dynamic properties of rubber compounds. In this work, two strong nano-scale materials, aramid nanofibers (ANFs) and graphene oxides (GOs), are modified using a silane coupling agent and combined to form a novel hybrid filler. The functionalized ANF/GO (fANF/GO) hybrid filler is obtained by adding functionalized GOs (fGOs) into functionalized ANFs (fANFs). The fANF/GO reinforced rubber compounds are then fabricated and tested to investigate the effect of the novel hybrid filler on mechanical and dynamic mechanical properties. The prepared rubber compounds using hybrid fillers exhibit improved mechanical properties and abrasion resistance compared to rubber compounds only reinforced using fANF or fGO alone and reference compounds. Moreover, dynamic mechanical analysis reveals a 21.8% decrease in the rolling resistance of fANF/GO reinforced rubber samples while preserving wet grip performance. Thus, this research demonstrates the potential of the ANFs and GOs-based functionalized hybrid fillers for the application of high-performance tire treads.

KEYWORDS

aramid nanofibers, mechanical properties, nanocomposite, rubber, viscosity and viscoelasticity, tire

1 | INTRODUCTION

Tires used in passenger vehicles are designed to operate in a safe and energy-efficient manner, which requires them to maintain excellent performance under various conditions, such as high grip on wet and dry roads, low rolling resistance, and a long lifespan. In order to achieve such a performance, wet skid resistance, fuel efficiency, and abrasion resistance are the most emphasized properties, forming what is known as “magic triangle” of tire technology.^{1,2}

However, it remains difficult to simultaneously maximize these properties due to them being interrelated to each other, as an increase in one usually causes a decrease in the other two. The previously mentioned properties are mostly affected by the characteristics of rubber compounds for tire tread, which can be heavily dictated by choice of reinforcing nanofiller. Therefore, to meet the performance requirements for tire tread compounds, researchers have relied on fillers, including carbon black,³ silica,^{4,5} graphene oxides,^{6–9} carbon nanotubes,^{10–12} nano clays,^{13,14} and nanofibers^{15–18}

to act as nanoscale reinforcement. Specifically, carbon black and silica have been commonly used in the industry for reinforcing rubber compounds. However, increasing the amount of carbon black causes high rolling resistance, while silica-filled rubber compounds require well-controlled mixing processes to achieve a comparable abrasion resistance to the carbon black filled rubber.^{19,20} Given the described disadvantages, recent research efforts have focused on exploring the role of novel nano-sized organic materials as promising fillers in rubber compounds and their potential in practical applications.

Graphene oxides (GOs) have attracted wide interest due to their excellent mechanical properties and large surface area, along with their high thermal stability and electrical conductivity.^{21–24} Because of their outstanding properties, GOs have been used as a nanoscale reinforcement in elastomers. For example, Mao et al. fabricated GO/styrene-butadiene rubber (SBR) nanocomposites through the mixing of GO colloid with SBR latex and butadiene-styrene-vinyl-pyridine rubber latex.²⁵ The 2 vol% GOs reinforced GO/SBR composites were found to exhibit comparable mechanical strength to that of SBR composites containing 13.1 vol% carbon black. Wu et al. also reported natural rubber (NR) nanocomposites reinforced with surface functionalized GOs using bis(triethoxysilylpropyl) tetrasulfide (TESPT).⁷ The functionalization of GOs with TESPT improved their dispersion in the NR matrix and contributed to a 100% and 66% increase in the ultimate strength and moduli of the resulting NR nanocomposites, in addition to a 48% reduction in their air permeability.

Aramid nanofibers (ANFs) are another type of organic nanomaterial that has shown great potential as a reinforcing filler in polymer matrices due to their outstanding mechanical properties, high surface area, and aspect ratio. First reported by Yang et al., ANFs are obtained through the dissolution and deprotonation of macroscale aramid fibers in a solution with dimethyl sulfoxide (DMSO) and potassium hydroxide (KOH).²⁶ Due to their excellent mechanical properties, ANFs have been used both to prepare nanocomposites based on polar matrices such as epoxy resin,^{27,28} polyurethane,²⁹ poly(acrylic acid),³⁰ poly(vinyl alcohol),^{31,32} and poly(methyl methacrylate) (PMMA)³³ and to reinforce non-polar rubber matrices. Chen et al. altered the surface chemistry of ANFs using epichlorohydrin and mixed them using a latex co-coagulation method to reinforce SBR.³⁴ Zhang et al. also used the same method to modify ANFs and then incorporated them into carboxylated acrylonitrile butadiene rubber (XNBR).³⁵ The modified ANF reinforced SBR and XNBR exhibited considerable improvement in their mechanical properties compared to pure SBR and XNBR, respectively. Moreover, TESPT functionalization was used to improve the dispersion

and interfacial interaction of ANFs with a rubber matrix.¹⁷ Our previous work has shown that the functionalized ANFs can be well dispersed in rubber matrix using a simple dry mixing method, yielding new rubber compounds with improved mechanical properties as well as abrasion resistance and fuel-saving efficiency without sacrificing performance in other metrics. The described work demonstrates the potential of functionalized ANFs as a promising nanofiller for tire tread rubber compounds.

Recently, the combination of two strong nanomaterials and the synergistic effect of the hybrid materials on the properties of polymer matrices have been reported. For example, Song prepared hybrid fillers based on two geometrically dissimilar fillers, including clay platelets and carbon nanotubes, and then used them to fabricate SBR nanocomposites with improved tensile strength, elastic modulus, and both thermal and electrical conductivities.³⁶ Moreover, the synergistic effect of multi-walled carbon nanotubes and graphene nanofillers on the mechanical performance of silicone rubber was also reported by Pradhan et al.³⁷ The hybrid filler reinforced nanocomposites exhibited 110% and 173% improvements in tensile strength and elastic modulus, respectively. Additionally, Fan et al. introduced ANFs into graphene nanosheets through $\pi - \pi$ stacking interactions and used the hybrid fillers to reinforce a PMMA matrix.³³ The 0.7 wt% ANF/GO hybrid nanofillers reinforced PMMA was shown to experience 84.5% and 70.6% increased tensile strength and modulus, respectively, exceeding any improvements observed in ANF or GO reinforced PMMA. These results confirm the potential of ANFs and GOs hybrid nanofillers for the reinforcement of rubber compounds.

In this study, ANFs and GOs are modified using TESPT and then combined to prepare a functionalized ANF/GO (fANF/GO) hybrid filler to reinforce rubber compounds. The fANF/GOs are predicted to yield greater improvements in the mechanical performance of rubber compounds compared to the reference compound, as well as ANF or GO reinforced rubber compounds. These improvements are attributed to the covalent bonding between fANF/GOs and rubber matrix and the noncovalent interaction between the ANFs and GOs. The prepared fANF/GO hybrid filler is characterized using Fourier transform infrared spectroscopy (FTIR), X-ray diffraction (XRD), ultraviolet–visible spectroscopy (UV–vis), and atomic force microscopy (AFM), while the mechanical performance of the fANF/GO reinforced rubber compound is assessed using tensile and abrasion resistance testing. Finally, dynamic mechanical analysis (DMA) is performed in order to predict the wet skid resistance and rolling resistance of the fANF/GO reinforced rubber compounds.

2 | EXPERIMENTAL SECTION

2.1 | Preparation of fANF/GO hybrid filler

ANF/DMSO suspensions were prepared using the method developed by Yang et al.²⁶ A mixture consisting of Kevlar® (2 g, CS-800), KOH (3 g, Fisher Scientific), and DMSO (1000 ml, Fisher Scientific) was stirred for 7 days at 25°C until an ANF suspension is formed. In order to functionalize the ANFs' surfaces, 10 wt% of TESPT (provided by Evonik) was added to the prepared suspension, which was then stirred at 80°C for 24 h. Concurrently, GOs were synthesized using the modified Hummer's method using a preoxidized graphite precursor.³⁸ The prepared GOs (2 g) were dispersed in DMSO (500 ml), followed by the addition of 10 wt% of TESPT, and then stirring at 80°C for 24 h. The functionalized GO/DMSO solution and the functionalized ANF/DMSO solution were combined and stirred at room temperature for 4 h to

prepare functionalized ANF/GO hybrid filler (fANF/GO) (Figure 1).

An equivalent amount of deionized water to DMSO was added to the final mixture to isolate the fANF/GOs, which were then collected using a vacuum-assisted filtration process. The fANF/GOs were then washed with deionized water and acetone several times to neutralize the highly basic solution and remove any unreacted chemicals. The obtained fANF/GOs were dispersed in water using sonication (Fisher Scientific Sonic Dismembrator Model 500) and then slightly dried to form an fANF/GO paste with 90 wt% water content. Functionalized ANFs (fANFs) and functionalized GOs (fGOs) were also prepared using the previously described procedures for comparison.

2.2 | Preparation of rubber compounds

A Brabender Plasti-corder internal mixer was used to prepare the fANF/GO reinforced rubber compounds according

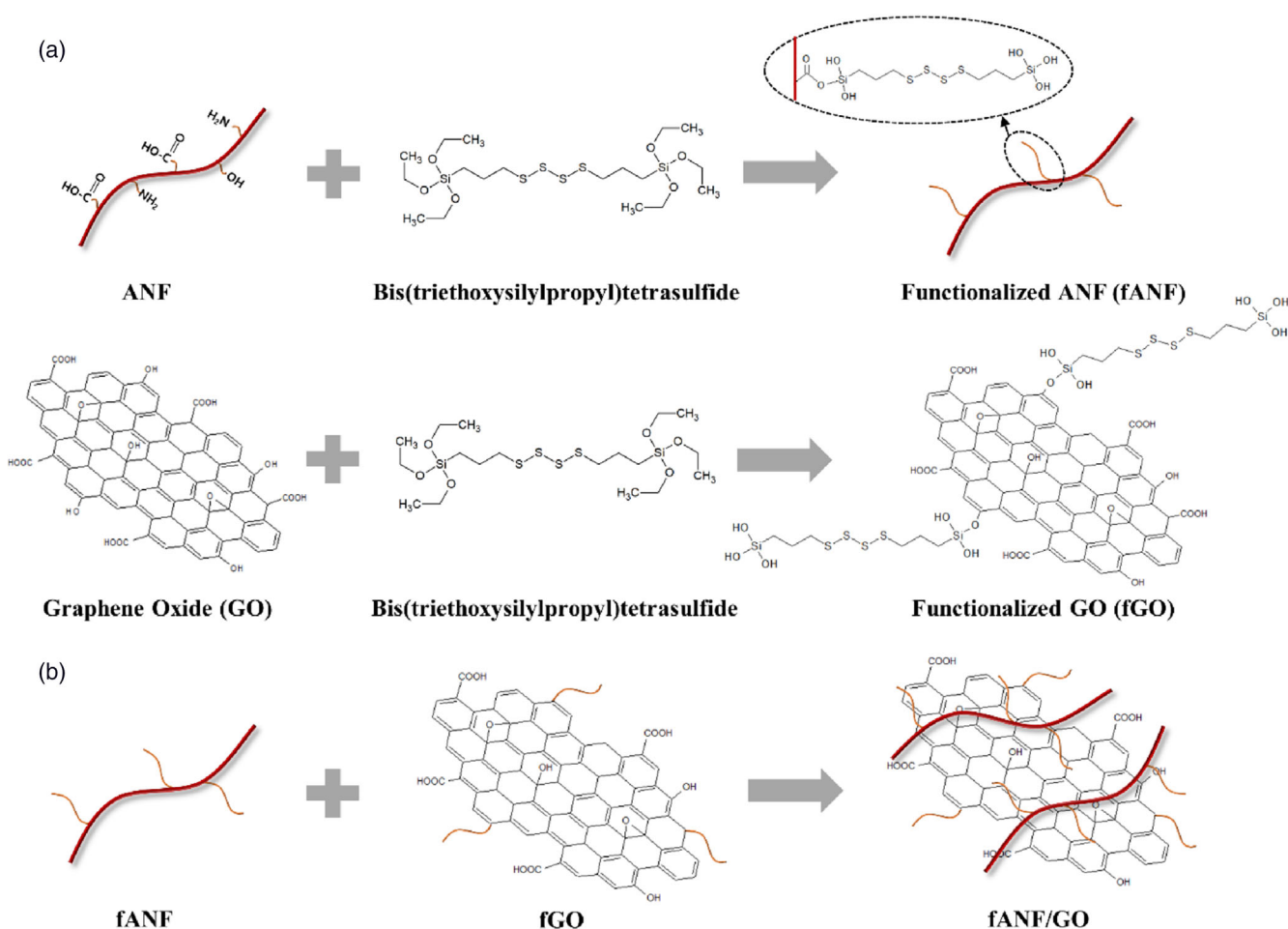


FIGURE 1 Illustration of the preparation of (a) fANF and fGO, and (b) fANF/GO hybrid filler [Color figure can be viewed at wileyonlinelibrary.com]

| Ingredients | Reference | 0.3 | 0.7 | 1 | 2 | 3 |
|-----------------------|-----------|-------|-------|-------|-------|-------|
| SOL-6270 M | 96.25 | 96.25 | 96.25 | 96.25 | 96.25 | 96.25 |
| KBR01 | 30 | 30 | 30 | 30 | 30 | 30 |
| N339 | 50 | 49.7 | 49.3 | 49 | 48 | 47 |
| fANF, fGO, or fANF/GO | — | 0.3 | 0.7 | 1 | 2 | 3 |
| Naphthenic oil | 3.75 | 3.75 | 3.75 | 3.75 | 3.75 | 3.75 |
| Zinc oxide | 3 | 3 | 3 | 3 | 3 | 3 |
| Stearic acid | 1 | 1 | 1 | 1 | 1 | 1 |
| Sulfur | 1.5 | 1.5 | 1.5 | 1.5 | 1.5 | 1.5 |
| CBS | 2.2 | 2.2 | 2.2 | 2.2 | 2.2 | 2.2 |

TABLE 1 Recipes of reference, fANF, fGO, and fANF/GO reinforced rubber compounds (unit: Phr, part per hundred parts of rubber)

to the recipes presented in Table 1. The rubber compounding was conducted at fill factors of 70% and temperatures ranging between 145 and 150°C. In the first stage, SBR SOL-6270 M (containing 37.5 parts of treated distillate aromatic extract oil, received from KKPC) and butadiene rubber KBR 01 (received from KKPC) were added to the mixer and blended for 1 min, before introducing carbon black (N339, provided by Birla Carbon), zinc oxide (received from Akrochem), stearic acid (received from Akrochem), and naphthenic oil (received from R.E. Carroll), followed by mixing for an additional 1 min. Then, fANF/GO was added to the rubber compound and mixed for an additional 5 min. The evaporation of water in the fANF/GO hybrid nanofiller was confirmed by the weight of the dumped mixture. In the second stage, sulfur and n-cyclohexyl-2-benzothiazole sulfonamide (CBS, received from Akrochem) were added to the original mixture and then mixed for 3 min prior to vulcanization using a hot press. The cure characteristics of rubber compounds were obtained using a Monsanto MDR 2000 at 160°C for 40 min.

2.3 | Characterization and tests

The chemical compositions of the fANF, fGO, and fANF/GO before and after functionalization were characterized by attenuated total reflectance–FTIR (ATR-FTIR), which was performed on a spectrometer (Nicolet iS60) equipped with a SMART iTR accessory. XRD patterns were monitored using CuK α radiation ($\lambda = 0.154$ nm) on an X-ray diffractometer (Rigaku Ultima IV). UV–vis spectrophotometer (PerkinElmer Lambda 950) was used to obtain UV–vis spectra in the range between 250 and 800 nm. AFM (Park AFM XE-70) was used to characterize the dimension and morphology of the fANF/GO. The abraded surfaces of rubber compound samples were also observed using a JEOL JSM-7800FLV field-emission scanning electron microscope (FE-SEM).

The crosslink density was measured and calculated through the swelling method using toluene according to the

procedure described elsewhere.¹⁷ Additionally, both tensile testing and dynamic mechanical analysis were performed on the reference and functionalized fillers reinforced compounds to investigate the effect of these fillers on their mechanical properties. Tensile testing was performed using an Instron universal load frame (Model 5982) at room temperature, where dumbbell-shaped specimens (ASTM D412 type C) were loaded at a 500 mm/min crosshead speed until failure. Viscoelastic properties were also determined in tensile mode using a DMA (TA Q800). Specimens with dimensions of 40.0 \times 6.0 \times 2.0 mm were mechanically loaded in air at 10 Hz, 0.5% strain, and a constant heating rate of 3°C min⁻¹ and temperatures ranging between -60 and 60°C. The abrasion resistance was evaluated using a DIN abrasion tester (Aveno Technology) according to the DIN 53516 standard. Specimens with dimensions of 16 mm in diameter and 8 mm in thickness were prepared and abraded on a cylinder-type drum rotating at a speed of 40 rpm. The weight of the sample was measured before and after the abrasion, and Equation (1) was used to calculate the abrasion loss.

$$A_A = \frac{\Delta m_t \times S_0}{d_t \times S} \quad (1)$$

where A_A is the loss from the abrasion (mm³), Δm_t is the loss in mass (mg), d_t is the compound's density (g cm⁻³), S is the abrasive grade (mg), and S_0 is the nominal abrasive grade (200 mg).

3 | RESULTS AND DISCUSSION

3.1 | Characterization of fANF/GO hybrid fillers

ATR-FTIR was used to characterize the surface functionalization of ANFs and GOs and the combination of the two fillers. The FTIR spectra of fANFs, fGOs, and fANF/GOs before and after the functionalization and

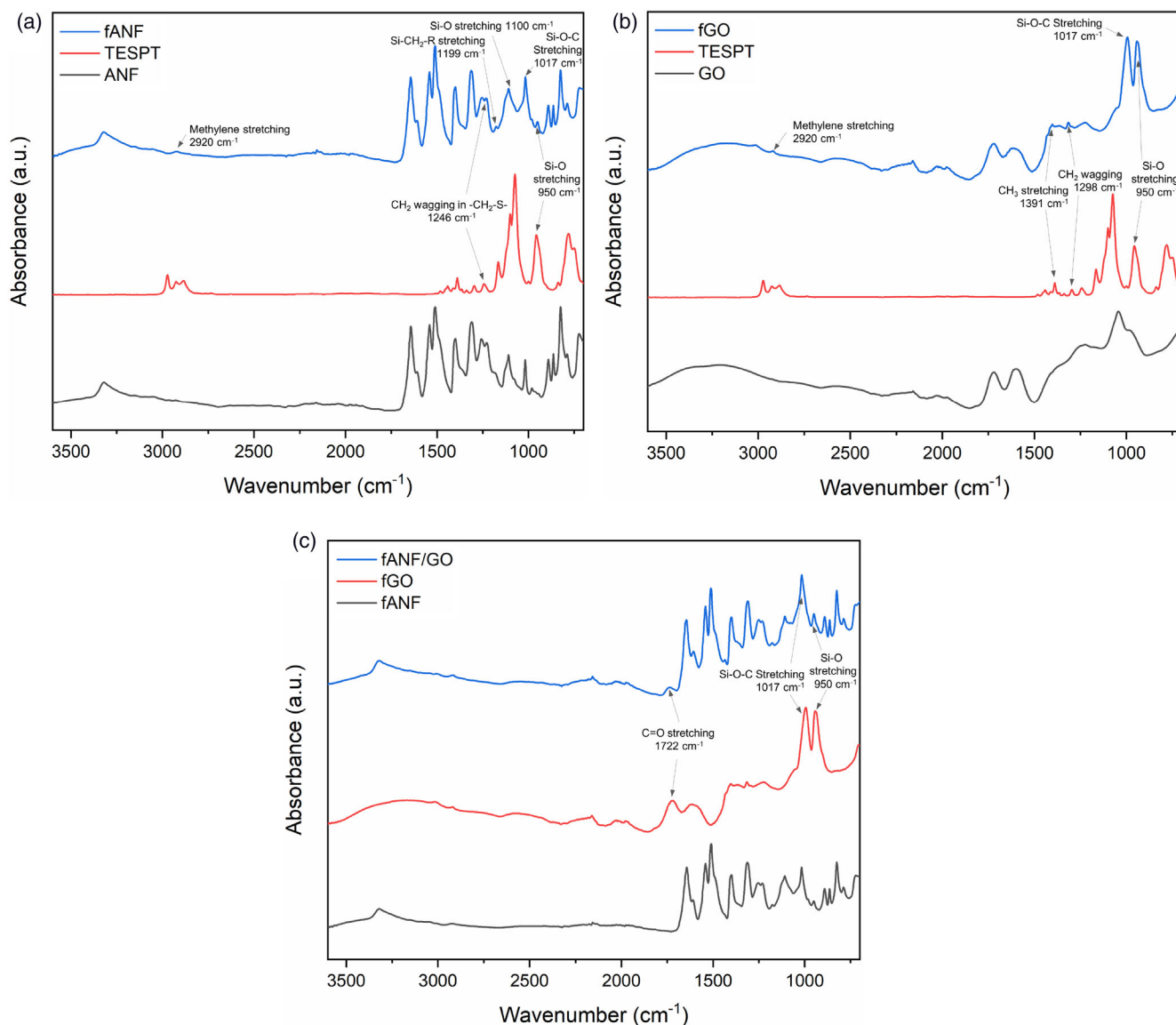


FIGURE 2 FTIR spectra of (a) fANFs, (b) fGOs, and (c) fANF/GOs [Color figure can be viewed at wileyonlinelibrary.com]

combination are shown in Figure 2. The characteristic peaks displayed by ANFs after the dissolution of aramid fibers are consistent with those previously reported.^{17,28,39,40} From the results in Figure 2a, the functionalization of the ANFs was confirmed based on the appearance of new characteristic peaks. Following functionalization, a peak at 2920 cm^{-1} corresponding to the methylene stretching vibration in the TESPT is observed in the fANFs' FTIR spectrum. The peaks at 1246 , 1199 , 1100 , 1017 , and 950 cm^{-1} are also attributed to the CH_2 wagging in $-\text{CH}_2-\text{S}-$, $\text{Si}-\text{CH}_2-\text{R}$, $\text{Si}-\text{O}$, $\text{Si}-\text{O}-\text{C}$, and $\text{Si}-\text{O}$ stretching vibration, respectively, as a result of functionalization. Similar to fANFs, fGOs display a new methylene stretching vibration peak at 2920 cm^{-1} post-functionalization, as shown in Figure 2b. In addition to the new peak, the fGOs display CH_3 stretching, CH_2 wagging, $\text{Si}-\text{O}-\text{C}$, and $\text{Si}-\text{O}$ stretching vibration peaks at 1391 , 1298 , 1017 , and 950 cm^{-1} , respectively, after

treatment. These new representative peaks confirm the introduction of a silane coupling agent on the surface of both ANFs and GOs. Once functionalized, both fANFs and fGOs were combined to obtain the fANF/GO hybrid fillers, which were subsequently characterized using FTIR. As seen in Figure 2c, the fANF/GOs FTIR spectra display the main characteristic peaks of both fANFs and fGOs. Thus, the chemical structural changes detected by FTIR confirm the functionalization of the ANFs and GOs in addition to their successful combination to form a new hybrid nanofiller.

The structure of the combined fillers was also characterized using XRD analysis and is shown in Figure 3a. Due to the crystalline structure of Kevlar, the XRD patterns of both ANFs and fANFs display the characteristic peaks at 20.6° and 22.9° , corresponding to the 110 and 200 planes of Kevlar, respectively.^{26,41} In contrast, GOs show a sharp characteristic peak at 12.8° with a d-spacing

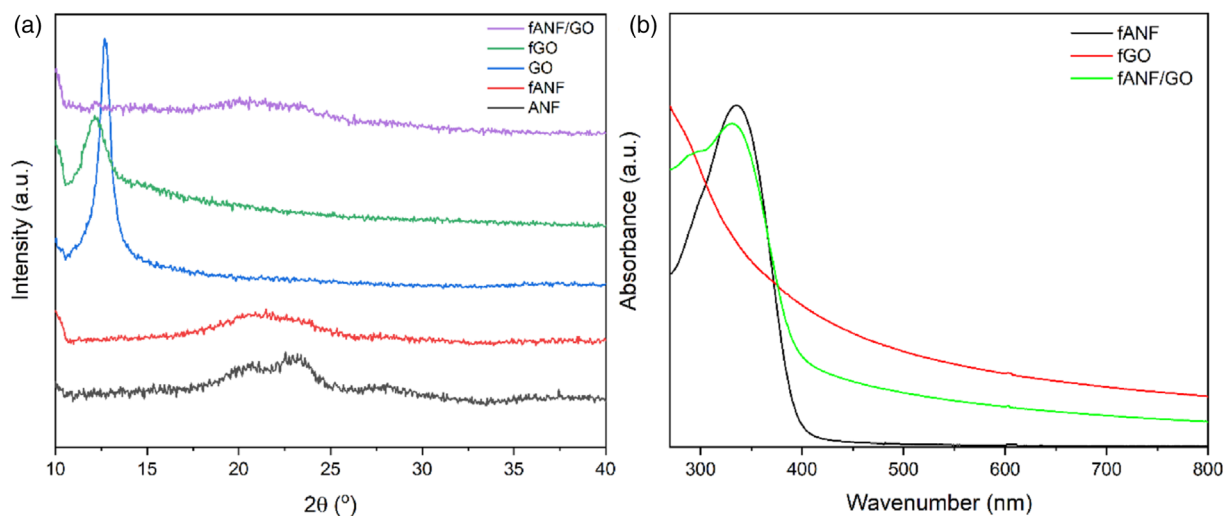


FIGURE 3 (a) XRD patterns of ANFs, fANFs, GOs, fGOs, and fANF/GOs and (b) UV-vis spectra of fANFs, fGOs, and fANF/GOs [Color figure can be viewed at wileyonlinelibrary.com]

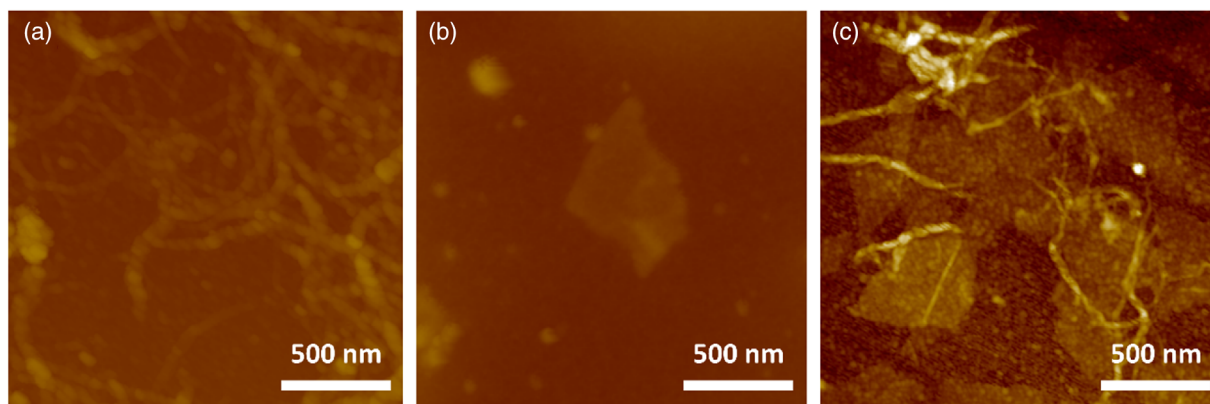


FIGURE 4 AFM scans of (a) fANFs, (b) fGOs, and (c) fANF/GOs [Color figure can be viewed at wileyonlinelibrary.com]

of 0.69 nm. However, the characteristic peak was observed to shift to 12.1° post-TESPT functionalization, corresponding to a d-spacing of 0.74 nm. These results confirm the disruption of interlayer packing of GOs through functionalization.⁷ Once fANFs and fGOs are combined, a small peak at 12.1° is observed, which is attributed to the characteristic peak of fGOs. Moreover, two peaks are also found at 20.6° and 22.9° , corresponding to the characteristic peaks of fANFs. The UV-vis spectra were also used to confirm the preparation of the fANF/GOs. As seen in Figure 3b, fANFs, fGOs, and fANF/GOs all show a shoulder peak near 300 nm, which is attributed to the tetrasulfide in the TESPT.⁴² Moreover, the ANF characteristic absorption peak at 335 nm is present in both the UV-vis spectra of fANFs and fANF/GOs.^{26,33} These UV-vis spectra thus confirm the combination of fANFs and fGOs, and the functionalization of the hybrid fillers. Additionally, AFM scans shown in Figure 4 provide further information on the morphology and dimensions of fANFs, fGOs, and fANF/GOs. The diameters of fANFs are

measured to range between 5 nm and 12 nm, which is consistent with previously reported studies,^{17,28} while the thickness of fGOs is measured to be 1.6 nm, which is in good agreement with the results reported by Wu et al.⁷ Furthermore, AFM scans of fANF/GOs indicate that fANFs are located on the surface and edge of fGOs, which confirms the interaction between them. Drawing from the FTIR, XRD, UV-vis, and AFM results, fANF/GOs can be considered as a hybrid filler that combines fANFs and fGOs through noncovalent interactions. The new hybrid filler can be useful for the reinforcement of the rubber matrix by establishing covalent bonding between the matrix and fillers, in addition to the noncovalent interfacial interactions between fANFs and fGOs.

3.2 | Mechanical properties

The mechanical properties of fANF, fGO, and fANF/GO reinforced rubber compounds were determined using

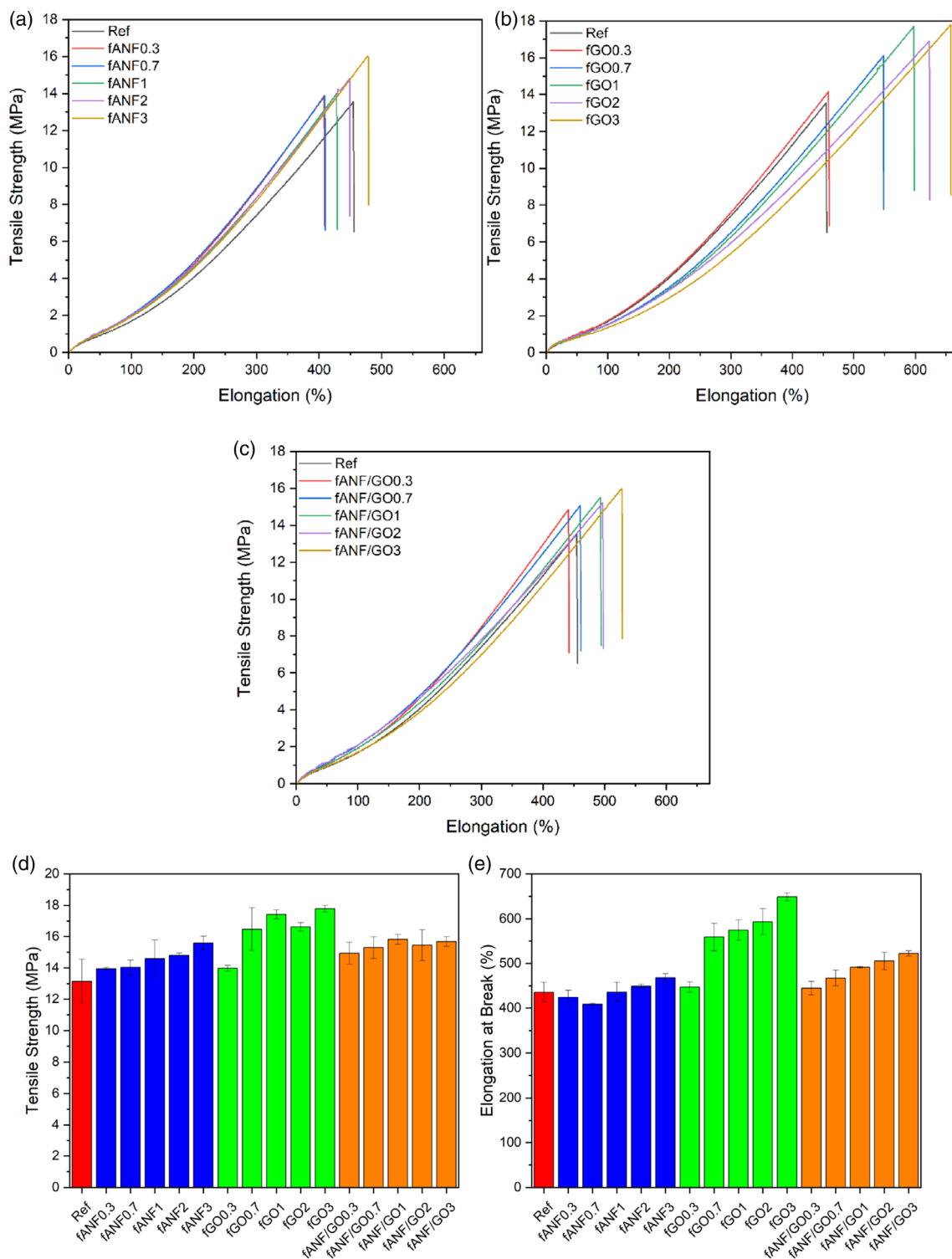


FIGURE 5 Stress–strain curves of (a) fANF0.3 to fANF3 samples, (b) fGO0.3 to fGO3 samples, and (c) fANF/GO0.3 to fANF/GO3 samples, and (d) tensile strength and (e) elongation at break of samples [Color figure can be viewed at wileyonlinelibrary.com]

tensile testing. Table S1 shows the average modulus at 100% and 300% elongation, tensile strength, and elongation at break of the rubber compounds, while their corresponding stress–strain curves are displayed in Figure 5. According to the tensile test results, fANF, fGO,

and fANF/GO are found to be a viable alternative to carbon black due to their capability of improving the mechanical properties of rubber compounds. Despite all the prepared compounds having the same filler loading of 50 phr, the average tensile strength and elongation at

break were found to be improved when incorporating fANF, fGO, and fANF/GO hybrid fillers. Specifically, fGO reinforced samples were found to exhibit a maximum tensile strength and elongation at break of 17.78 MPa and 648.9%, yielding 35.3% and 48.9% improvements compared to the reference compound, respectively. However, the 100% and 300% moduli of fGO

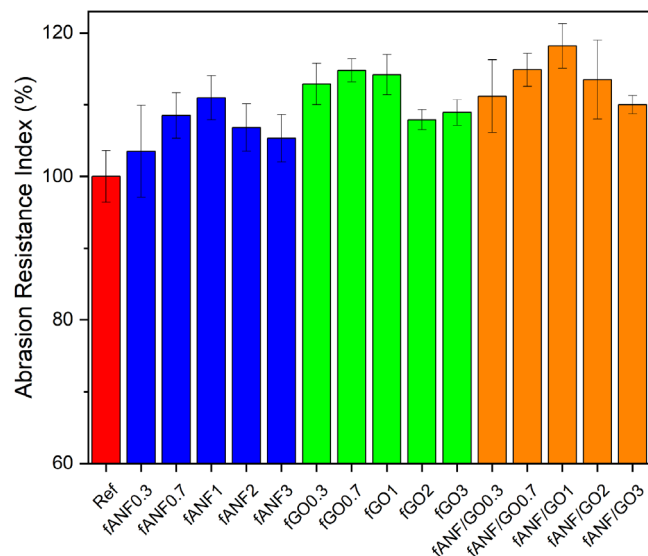


FIGURE 6 Abrasion resistance indexes of rubber compounds reinforced with fANFs, fGOs, and fANF/GOs [Color figure can be viewed at wileyonlinelibrary.com]

reinforced rubber compounds were found to display a decreasing trend with increasing fGO content in compounds. In contrast, the moduli of rubber compounds reinforced with 0.3 to 3 phr of fANFs were found to be higher than those of the reference compound, yet their elongation at break was measured to be decreased compared to fGO reinforced samples. Given the contrast in mechanical performance, the overall tensile properties of fANF/GO hybrid filler reinforced rubber samples were found to be approximately a combined average of those of fANF and fGO reinforced rubber samples. When compared to reference compounds, the fANF/GO reinforced rubber compounds displayed improved tensile strength, 100 and 300% moduli, and elongation at break, therefore suggesting that a comprehensive reinforcement effect of fANF/GO in the rubber. According to the tensile testing results, these new hybrid fillers outperform carbon black when it comes to improving the mechanical properties of rubber compounds. These results can be explained by examining the unique characteristics of both fANFs and fGOs. As investigated in our previous work, the large specific area and high aspect ratio of fANFs, along with their excellent strength and stiffness derived from their aramid molecular structure, can significantly contribute to reinforcing the rubber matrix.¹⁷ Similarly, fGOs also have an extraordinarily high specific surface area and mechanical properties, which are beneficial for their performance as nano-reinforcement.^{7,9,24} In addition to their physical characteristics, the strong interfacial interactions between

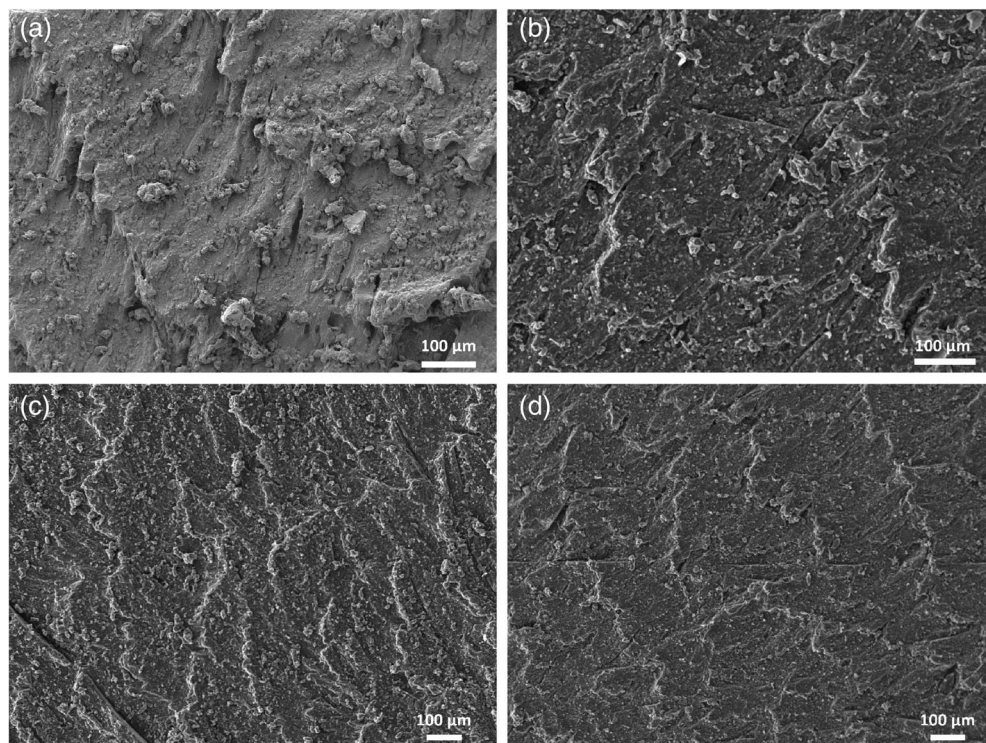


FIGURE 7 SEM images of abraded surfaces. (a) Reference compound sample, (b) fANF1 sample, (c) fGO1 sample, and (d) fANF/GO1 sample

these nanofillers and the rubber matrix through covalent linkage afforded by the silane coupling agent can also yield improvement in the overall mechanical properties, as proven by previous works.^{7,17} The enhancement of the interaction between the fillers and rubber matrix can also be confirmed using crosslink density measurements in the rubber samples, which are detailed in Table S1. As the concentration of fANFs, fGOs, and fANF/GOs in the rubber compounds is increased, the calculated crosslink density is also observed to increase. The crosslink densities of fGO reinforced rubber samples were found to be higher than those of the reference samples, fANF and fANF/GO reinforced rubber samples, which is in agreement with the previously discussed trend in tensile strength. This enhancement of crosslink density can be attributed to the characteristics of the new fillers that can contribute to improving load and stress transfer within the rubber matrix through the chemical covalent bonding.

3.3 | Abrasion resistance

In addition to the tensile properties, the abrasion resistance of fANF, fGO, and fANF/GO reinforced rubber compounds was studied using abrasion resistance testing. The collected measurements were converted to abrasion resistance indexes by determining the ratio of abrasion loss of the reference compound to that of the nano-reinforced specimens. Figure 6 shows the test results of rubber compounds reinforced with 50 phr of total fillers, including 0.3 to 3 phr of new fillers. When examining test results, it can be seen that the fANF, fGO, and fANF/GO reinforced samples all showed improved abrasion resistance in comparison to that of the reference sample. Upon adding 1 phr of new fillers, the average abrasion resistance of the fANF, fGO, and fANF/GO reinforced samples displayed 11.0%, 14.2%, and 18.2% improvements, respectively. These test results suggest that the new functionalized fillers can enhance the abrasion

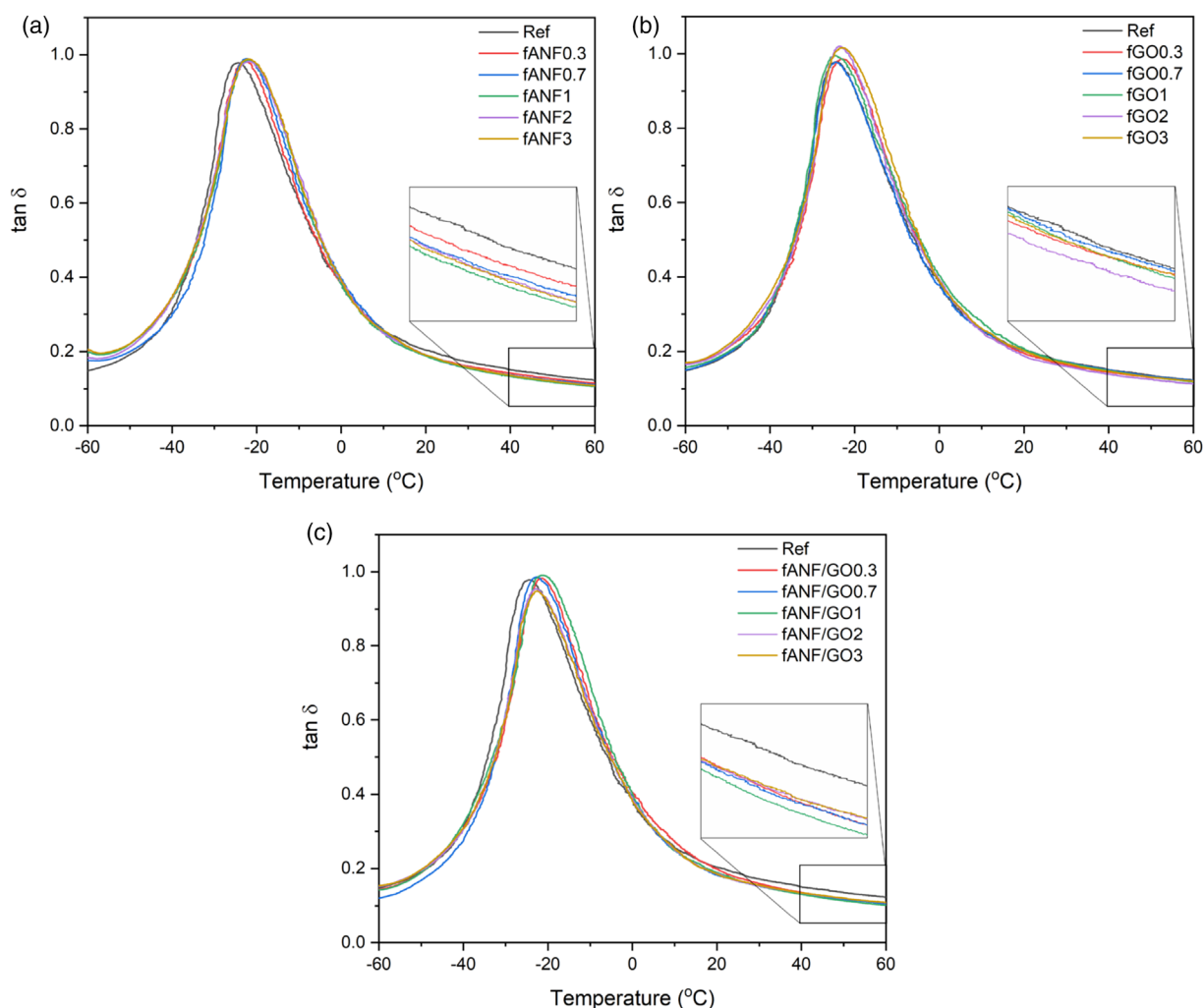


FIGURE 8 tan δ curves of (a) fANF0.3 to fANF3 samples, (b) fGO0.3 to fGO3 samples, and (c) fANF/GO0.3 to fANF/GO3 samples [Color figure can be viewed at wileyonlinelibrary.com]

resistance of rubber compounds, which is in agreement with the improved mechanical strength and toughness of these compounds previously concluded from tensile testing and crosslink density measurements. Moreover, the maximum abrasion resistance displayed by fANF/GO reinforced rubber compounds highlights the synergetic effect of the fANFs and fGOs for the reinforcement of the rubber matrix. This can be explained by the interaction between the fANFs and fGO, which reduces the stress concentrations in the rubber matrix by transferring it from the fANFs to the surface of fGOs.³³ Following abrasion resistance testing, the abraded surfaces of rubber compounds were examined using SEM imaging in order to further understand the effect of new fillers on rubber abrasion, and are shown in Figure 7. Post-abrasion, ridges were formed on the abraded rubber surfaces due to the detachment of abraded particles. While the abraded surface of the reference sample shows a rough texture, the abraded surfaces of fANF, fGO, and fANF/GO reinforced samples clearly display a considerable decrease in roughness. A large amount of debris and higher ridges were observed on the abraded surface of the reference compound, which corresponds to the high abrasion volume.^{25,43} However, relatively lower ridges were formed on the surface of compounds reinforced with new fillers, showing low abrasion loss. Therefore, the observed characteristics of the abraded surfaces correlate well with the abrasion resistance test results.

3.4 | Dynamic mechanical analysis

In addition to tensile and abrasion resistance testing, the viscoelastic performance of the fANF/GO reinforced rubber compounds was examined by performing dynamic mechanical analysis. The viscoelastic properties of rubber compounds are important because they can be used to predict tire performance metrics such as wet traction and fuel efficiency.^{44–46} Specifically, the values of $\tan \delta$ at 0 and 60°C are usually representative for the prediction of wet grip performance and fuel-saving efficiency: the higher $\tan \delta$ value at 0°C, the better wet grip performance, while the lower $\tan \delta$ value at 60°C, the lower rolling resistance which corresponds to better fuel-saving efficiency. The resulting $\tan \delta$ curves are presented in Figure 8, and the values of $\tan \delta$ at 0 and 60°C are shown in Table 2. The fANF reinforced samples displayed increased fuel-saving efficiency and comparable wet grip performance to reference compounds, which is in agreement with the trend shown in our previous work using the fANFs.¹⁷ In contrast, the improvement in fuel efficiency was not significant for fGO reinforced rubber compounds, and wet grip performance remained comparable

TABLE 2 DMA results of fANF, fGO, and fANF/GO reinforced rubber samples

| Parameters | $\tan \delta$ at 0°C | $\tan \delta$ at 60°C |
|------------|----------------------|-----------------------|
| Reference | 0.386 | 0.123 |
| fANF0.3 | 0.383 | 0.115 |
| fANF0.7 | 0.398 | 0.111 |
| fANF1 | 0.382 | 0.106 |
| fANF2 | 0.391 | 0.109 |
| fANF3 | 0.391 | 0.108 |
| fGO0.3 | 0.391 | 0.120 |
| fGO0.7 | 0.379 | 0.122 |
| fGO1 | 0.402 | 0.119 |
| fGO2 | 0.393 | 0.114 |
| fGO3 | 0.391 | 0.120 |
| fANF/GO0.3 | 0.405 | 0.106 |
| fANF/GO0.7 | 0.391 | 0.106 |
| fANF/GO1 | 0.400 | 0.101 |
| fANF/GO2 | 0.395 | 0.108 |
| fANF/GO3 | 0.382 | 0.109 |

to reference compounds. However, the combination of fANFs and fGOs was clearly found to reduce rolling resistance through the synergetic effect. When rubber compounds were reinforced with fANF/GOs, the tire performance metric for the fuel-saving efficiency predicted by the ratio of $\tan \delta$ values was found to improve by up to 21.8% compared to reference compounds, outperforming the fANF reinforced samples. These results can be explained by the covalent bonding between the rubber matrix and new fillers and the improved interfacial interaction between the fANFs and fGOs. The rolling resistance of the carbon black reinforced rubber is a result of the repetitive breakdown and reformation of the rubber-carbon black and carbon black-carbon black interactions, which dissipate energy during deformation.^{47,48} The covalent bonding between the rubber matrix and the new fillers minimizes energy dissipation by preventing the breakdown and reformation of rubber-filler interaction.¹⁷ In addition to the covalent bonding, the interfacial interaction between the fANFs and fGOs can also contribute to the reduced energy dissipation, which subsequently leads to improved fuel efficiency. Additionally, the glass transition temperature, T_g , obtained from the maximum peak value of $\tan \delta$ is also found to be increased when fANFs and fANF/GOs were incorporated into the rubber compounds. It is known that the glass transition temperature of composite materials is related to the flexibility of polymer chains in the composites. Therefore, the T_g can be shifted to a higher

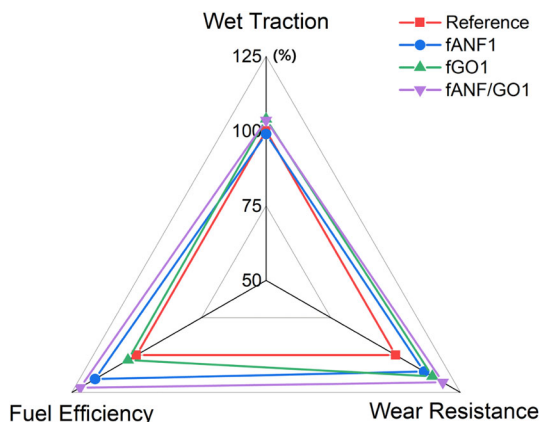


FIGURE 9 The “magic triangle” of tire performance indexes for fANF, fGO, and fANF/GO reinforced rubber compounds predicted by DMA and abrasion resistance results [Color figure can be viewed at wileyonlinelibrary.com]

temperature due to the restricted mobility of rubber molecules by the incorporation of fANFs and fANF/GOs into the rubber matrix.⁴⁹ Such results further confirm the improved interfacial interaction and crosslink density between the rubber matrix and new fillers. Deduced from the DMA and abrasion resistance test results, the “magic triangle” of tire performance for the fANF, fGO, and fANF/GO reinforced rubber compounds can be seen in Figure 9. The wet skid resistance and fuel-saving efficiency were predicted by the ratio of the reference compound and fANF, fGO, and fANF/GO reinforced compounds' $\tan \delta$ value at 0 and 60°C, respectively. Therefore, both fANFs and fGOs can yield improved fuel-saving efficiency and abrasion resistance in rubber compounds while preserving wet skid resistance. These improvements can be further amplified when using fANFs/GO nanofillers, as their synergetic effect in tire rubber compounds can result in further improvements in abrasion resistance and fuel-saving efficiency without compromising the wet grip performance.

4 | CONCLUSION

In this study, ANFs and GOs were modified using TESPT and then combined to prepare fANF/GO hybrid filler for the reinforcement of tire tread rubber compounds. The results of characterization using FTIR, XRD, UV-vis, and AFM confirmed that the fANFs and fGOs are combined through noncovalent interactions. Rubber compounds reinforced with fANFs, fGOs, and fANF/GOs were prepared and tested to investigate and compare the effect of the new fillers on the properties related to the tire tread

performances. Tensile testing results showed that fANF/GO reinforced rubber compounds exhibit improved average tensile strength and elongation at break relative to fANF reinforced samples, while also displaying higher moduli relative to fGO reinforced rubber compounds. The improvements of mechanical properties due to the new functionalized fillers were also supported by crosslink density measurement results. Moreover, the abrasion resistance of fANFs, fGOs, and fANF/GOs reinforced rubber compounds were found to be increased, with fANF/GO reinforced rubber samples displaying an 18.2% improvement in abrasion resistance upon adding 1 part of the fANF/GO hybrid filler. In addition to mechanical properties, DMA testing results showed that the rolling resistance predicted by $\tan \delta$ at 60°C was improved in fANF, fGO, and fANF/GO reinforced rubber compounds while maintaining the wet skid resistance. Most notably, 1 part of fANF/GOs reinforced rubber specimens showed 21.8% improvement in rolling resistance. Therefore, this study demonstrates that the new fANF/GO hybrid filler can increase mechanical properties and overall tire performance without resulting in a performance trade-off.

ACKNOWLEDGMENTS


This work was financially supported by Hankook tire and technology Co., Ltd, the Army Research Office through contract number W911NF-18-1-0061, and the Air Force Office of Scientific Research through Contract number FA9550-21-1-0019.

DATA AVAILABILITY STATEMENT

No. Research data are not shared.

ORCID

Jaehyun Jung  <https://orcid.org/0000-0001-9592-9338>

Henry A. Sodano  <https://orcid.org/0000-0001-6269-1802>

REFERENCES

- [1] P. Manoharan, K. Naskar, *J. Appl. Polym. Sci.* **2016**, *133*, 43531.
- [2] P. Thaptong, P. Sae-Oui, C. Sirisinha, *Rubber Chem. Technol.* **2017**, *90*, 699.
- [3] M. L. Studebaker, *Rubber Chem. Technol.* **1957**, *30*, 1400.
- [4] S. Mihara, R. N. Datta, J. W. M. Noordermeer, *Rubber Chem. Technol.* **2009**, *82*, 524.
- [5] K. E. Polmanteer, C. W. Lentz, *Rubber Chem. Technol.* **1975**, *48*, 795.
- [6] Z. Tang, X. Wu, B. Guo, L. Zhang, D. Jia, *J. Mater. Chem.* **2012**, *22*, 7492.
- [7] J. Wu, G. Huang, H. Li, S. Wu, Y. Liu, J. Zheng, *Polymer* **1930**, *2013*, 54.
- [8] W. Xing, H. Li, G. Huang, L. H. Cai, J. Wu, *Compos. Sci. Technol.* **2017**, *144*, 223.

- [9] Z. Yang, J. Liu, R. Liao, G. Yang, X. Wu, Z. Tang, B. Guo, L. Zhang, Y. Ma, Q. Nie, F. Wang, *Compos. Sci. Technol.* **2016**, *132*, 68.
- [10] A. Das, K. W. Stöckelhuber, R. Jurk, M. Saphiannikova, J. Fritzsche, H. Lorenz, M. Klüppel, G. Heinrich, *Polymer* **2008**, *49*, 5276.
- [11] H. H. Le, M. N. Sriharish, S. Henning, J. Klehm, M. Menzel, W. Frank, S. Wießner, A. Das, K. W. Stöckelhuber, G. Heinrich, H. J. Radusch, *Compos. Sci. Technol.* **2014**, *90*, 180.
- [12] Y. Lu, J. Liu, G. Hou, J. Ma, W. Wang, F. Wei, L. Zhang, *Compos. Sci. Technol.* **2016**, *137*, 94.
- [13] S. Praveen, P. K. Chattopadhyay, P. Albert, V. G. Dalvi, B. C. Chakraborty, S. Chattopadhyay, *Compos. Part A Appl. Sci. Manuf.* **2009**, *40*, 309.
- [14] J. Carretero-González, H. Retos, R. Verdejo, S. Toki, B. S. Hsiao, E. P. Giannelis, M. A. López-Manchado, *Macromolecules* **2008**, *41*, 6763.
- [15] J. Wu, X. Zhang, K. Jiang, H. Jia, X. Rui, F. Yang, *Fibers Polym.* **1808**, 2020, 21.
- [16] K. P. Surya, S. Bhattacharya, R. Mukhopadhyay, K. Naskar, A. K. Bhowmick, *Rubber Chem. Technol.* **2020**, *93*, 471.
- [17] J. Jung, H. A. Sodano, *ACS Appl. Polym. Mater.* **2020**, *2*, 4874.
- [18] M. Pingot, B. Szadkowski, M. Zaborski, *Polym. Adv. Technol.* **2018**, *29*, 1661.
- [19] J. T. Byers, *Rubber Chem. Technol.* **2002**, *75*, 527.
- [20] W. Kaewsakul, K. Sahakaro, W. K. Dierkes, J. W. M. Noordermeer, *Rubber Chem. Technol.* **2012**, *85*, 277.
- [21] C. Y. Lee, J. H. Bae, T. Y. Kim, S. H. Chang, S. Y. Kim, *Compos. Part A Appl. Sci. Manuf.* **2015**, *75*, 11.
- [22] Y. K. Kim, D. H. Min, *Carbon N.Y.* **2010**, *48*, 4283.
- [23] X. Li, W. Nie, Y. Xu, Y. Zhou, P. Chen, C. Zhang, *Compos. Part B Eng.* **2020**, *198*, 108234.
- [24] X. Liu, W. Kuang, B. Guo, *Polymer* **2015**, *56*, 553.
- [25] Y. Mao, S. Wen, Y. Chen, F. Zhang, P. Panine, T. W. Chan, L. Zhang, Y. Liang, L. Liu, *Sci. Rep.* **2013**, *3*, 1.
- [26] M. Yang, K. Cao, L. Sui, Y. Qi, J. Zhu, A. Waas, E. M. Arruda, J. Kieffer, M. D. Thouless, N. A. Kotov, *ACS Nano* **2011**, *5*, 6945.
- [27] J. Lin, S. H. Bang, M. H. Malakooti, H. A. Sodano, *ACS Appl. Mater. Interfaces* **2017**, *9*, 11167.
- [28] J. Jung, H. A. Sodano, *Polymer* **2020**, *195*, 122438.
- [29] Q. Kuang, D. Zhang, J. C. Yu, Y. W. Chang, M. Yue, Y. Hou, M. Yang, *J. Phys. Chem. C* **2015**, *119*, 27467.
- [30] M. Yang, K. Cao, B. Yeom, M. D. Thouless, A. Waas, E. M. Arruda, N. A. Kotov, *J. Compos. Mater.* **1873**, 2015, 49.
- [31] Y. Guan, W. Li, Y. Zhang, Z. Shi, J. Tan, F. Wang, Y. Wang, *Compos. Sci. Technol.* **2017**, *144*, 193.
- [32] L. Xu, X. Zhao, C. Xu, N. A. Kotov, *Adv. Mater.* **2018**, *30*, 1.
- [33] J. Fan, Z. Shi, L. Zhang, J. Wang, J. Yin, *Nanoscale* **2012**, *4*, 7046.
- [34] Y. Chen, Q. Yin, X. Zhang, W. Zhang, H. Jia, Q. Ji, F. Yang, X. Rui, *Compos. Part B Eng.* **2019**, *166*, 196.
- [35] X. Zhang, Y. Chen, Q. Yin, J. Wu, W. Song, A. Mohamed, H. Jia, F. Yang, X. Rui, *Mater. Chem. Phys.* **2019**, *238*, 121926.
- [36] S. H. Song, *Macromol. Chem. Phys.* **2016**, *217*, 2617.
- [37] B. Pradhan, S. K. Srivastava, *Polym. Int.* **2014**, *63*, 1219.
- [38] S. Stankovich, D. A. Dikin, R. D. Piner, K. A. Kohlhaas, A. Kleinhammes, Y. Jia, Y. Wu, S. B. T. Nguyen, R. S. Ruoff, *Carbon N.Y.* **2007**, *45*, 1558.
- [39] J. Nasser, J. Lin, H. Sodano, *J. Appl. Phys.* **2018**, *124*, 045305.
- [40] B. A. Patterson, M. H. Malakooti, J. Lin, A. Okorom, H. A. Sodano, *Compos. Sci. Technol.* **2018**, *161*, 92.
- [41] M. Lian, J. Fan, Z. Shi, H. Li, J. Yin, *Polymer* **2014**, *55*, 2578.
- [42] J. E. Baer, M. Carmack, *J. Am. Chem. Soc.* **1949**, *71*, 1215.
- [43] C. K. Hong, H. Kim, C. Ryu, C. Nah, Y. Huh, S. Kaang, *J. Mater. Sci.* **2007**, *42*, 8391.
- [44] E. Cichomski, W. K. Dierkes, T. V. Tolpekina, S. Schultz, J. W. M. Noordermeer, *KGK, Kautsch. Gummi Kunstst.* **2014**, *67*, 50.
- [45] R. R. Rahalkar, *Rubber Chem. Technol.* **1989**, *62*, 246.
- [46] G. Heinrich, *Rubber Chem. Technol.* **1997**, *70*, 1.
- [47] J. B. Donnet, *Rubber Chem. Technol.* **1998**, *71*, 323.
- [48] J. Han, X. Zhang, W. Guo, C. Wu, *J. Appl. Polym. Sci.* **2006**, *100*, 3707.
- [49] X. Cao, C. Xu, Y. Liu, Y. Chen, *Carbohydr. Polym.* **2013**, *92*, 69.

SUPPORTING INFORMATION

Additional supporting information may be found in the online version of the article at the publisher's website.

How to cite this article: J. Jung, H. A. Sodano, *J. Appl. Polym. Sci.* **2022**, *139*(13), e51856. <https://doi.org/10.1002/app.51856>